Manipulation of Surface-Tethered Helical Polypeptide-Based Nanostructures with Localized Chemical Functionalities

CNF Project Number: 1757-09
Principal Investigator(s): Christopher Kemper Ober
User(s): Yuming Huang

Affiliation(s): Department of Materials Science and Engineering, Cornell University

Primary Source(s) of Research Funding: National Science Foundation

Contact: cko3@cornell.edu, yh839@cornell.edu
Website(s): https://ober.mse.cornell.edu/index.html

Primary CNF Tools Used: E-beam Resist Spinners, JEOL 9500, FilMetrics F50-EXR, Oxford 81 Etcher, Zeiss Ultra SEM, Veeco Icon AFM, Optical Microscope, Oxford 81

Abstract:

Polymer brushes are polymer chains with one end covalently anchored to a surface. Due to the unusual molecular arrangements and surface attachments, these densely grafted polymer brushes have exhibited unique mechanochemical properties and thus have gained wide interest from the polymer science community. Potential applications of such thin film could be biosensors, photovoltaic devices, organic electronics, and biomimicry surfaces. It was previously reported that the arrangement of polymer brushes could be organized via an integrated process of electron beam lithography, surface-initiated synthesis, and post-processing treatments. In this work, the customizability of such polymer nanostructure was further enhanced by end-point functionalization and vapor annealing process.

Summary of Research:

Polymer brushes have demonstrated various responsive behaviors towards external stimuli such as solvents [1], pH [2], temperature [3], and ionic strength [4]. It has been found that polymer brushes can display novel behaviors when subjected to nanoconfinement [5]. Previously, we reported a nanopatterning process of making "spiky" nanoarrays of polypeptide rod brushes on silicon substrates which have resulted in interesting "bridging" morphology governed by the localized chain-chain interactions (Figure 1 and 2) [6]. However, the characterization and manipulation of the chain arrangement in these nanostructured brushes can be challenging due to the extremely small feature sizes (less than 100nm) and highly confined structure.

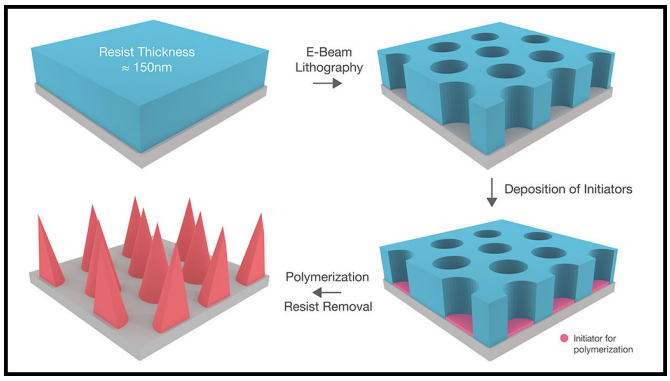

Figure 1: Schematic illustration of the fabrication process of nanopatterned brushes.

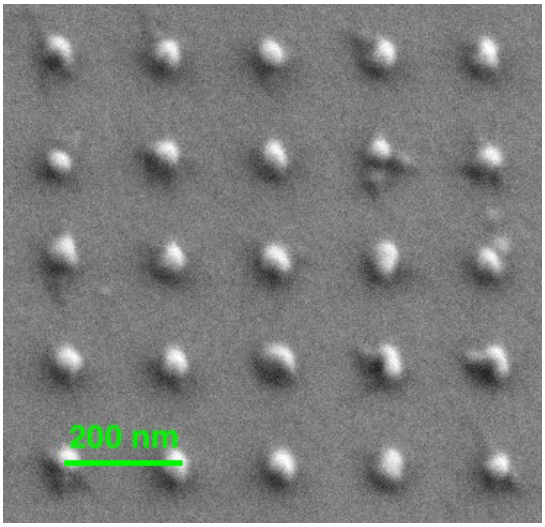

Figure 2: SEM image of the patterned PBLG rod brushes.

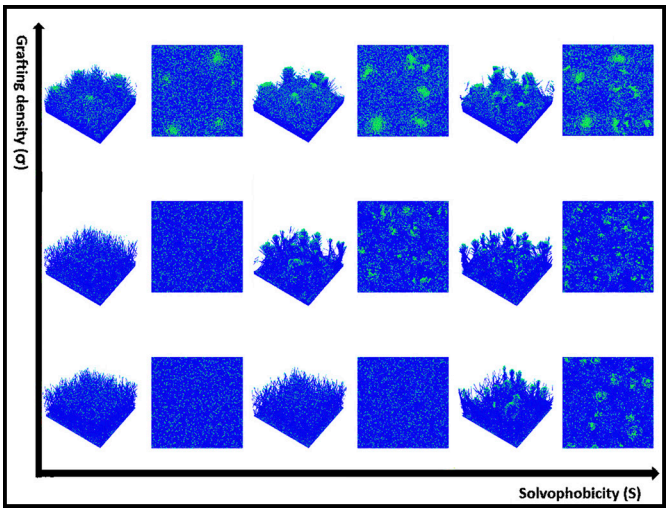

Figure 3: Computational simulation of rod brushes in various conditions.

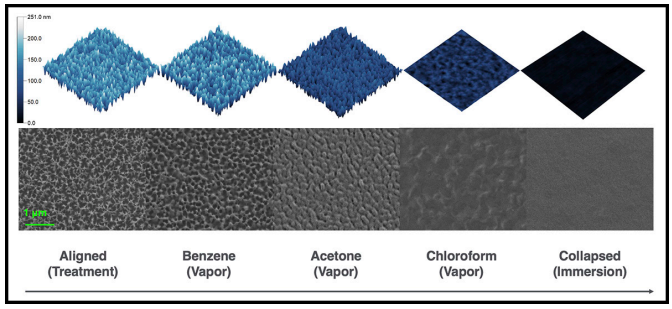

Figure 4: The SEM and AFM characterizations of PBLG brushes undergoing different treatments.

In this study, the organization of polypeptide rod brushes was examined via an integrated study of computational simulations and fluorescent dye-functionalized rod brushes. Chain-end functionalization of the brush tip was realized by chemically modifying the end groups with fluorescent probes — the fluorescence properties of the resulting brush film were found to be sensitive to the chain arrangement due to the aggregation-induced mechanism of the fluorophores. Coarse-grained rod polymer models, in conjunction with a density field-based energy function, were built to analyze the influence of various factors on the chain orientation, end-point density, and overall brush morphology (Figure 3).

Moreover, the potential of polypeptide rod brushes to serve as recognition elements in sensing devices for volatile organic compounds (VOCs) has been explored. The film's response to different VOCs, including benzene, chloroform, and acetone, was analyzed using an *in-situ* monitoring system based on reflectometry for real-time monitoring of vapor responses. It has been found that the brush exhibited reversible swelling-collapsing behavior when exposed to different VOCs such as benzene, chloroform, and acetone. Subsequently, a vapor treatment technique was developed to fine-tune the morphology of PBLG brushes, which has the potential to produce customizable nanostructured surfaces in combination with nanolithography (Figure 4).

In addition to nanolithography, we have demonstrated that polymer nanostructures can be further customized by chemical modification of the chain-ends and vapor-phase annealing process. The distribution and molecular arrangements of these active chain-ends can be examined by the behavior of the attached fluorescence molecules and controlled by vapor-phase treatment. In the future, we plan to explore the possibility of functionalizing these nanostructures with bioactive compounds for biomimicry surface and modeling study. We also plan to introduce mixed rod-coil brushes in the same system for binary and stimuli-responsive surface functionalities.

References:

[1] C.-T. Yang, Y. Wang, C. W. Frank, and Y.-C. Chang, "Chemoresponsive surface-tethered polypeptide brushes based on switchable secondary conformations," Rsc Adv, vol. 5, no. 105, pp. 86113-86119, 2015, doi: 10.1039/c5ra15839g.

[2] G. A. Eken, Y. Huang, Y. Guo, and C. Ober, "Visualization of the pH Response through Autofluorescent Poly(styrene-alt-Nmaleimide) Polyelectrolyte Brushes," Acs Appl Polym Mater, vol. 5, no. 2, pp. 1613-1623, 2023, doi: 10.1021/acsapm.2c02066.

[3] X. Wang, et al., "Temperature-Responsive Hierarchical Polymer Brushes Switching from Bactericidal to Cell Repellency," ACS Appl. Mater. Interfaces, vol. 9, no. 46, pp. 40930-40939, 2017, doi: 10.1021/acsami.7b09968.

[4] C.-H. Lin and S.-C. Luo, "Combination of AFM and Electrochemical QCMD for Probing Zwitterionic Polymer Brushes in Water: Visualization of Ionic Strength and Surface Potential Effects," Langmuir, vol. 37, no. 42, pp. 12476-12486, 2021, doi: 10.1021/acs.langmuir.1c02230.

[5] W.-L. Chen, M. Menzel, O. Prucker, E. Wang, C. K. Ober, and J. Rühe, "Morphology of Nanostructured Polymer Brushes Dependent on Production and Treatment," Macromolecules, vol. 50, no. 12, pp. 4715-4724, 2017, doi: 10.1021/acs.macromol.7b00714.

[6] Y. Huang, H. Tran, and C. K. Ober, "High-Resolution Nanopatterning of Free-Standing, Self-Supported Helical Polypeptide Rod Brushes via Electron Beam Lithography," Acs Macro Lett, vol. 10, no. 6, pp. 755-759, 2021, doi: 10.1021/acsmacrolett.1c00187.

Sequence-Defined Polypeptoid CARs for Electron-Beam and EUV Lithography

CNF Project Number: 1757-09
Principal Investigator(s): Christopher Kemper Ober
User(s): Florian Hermann Ulrich Kaefer, Chaoqiuyu Wang

Affiliation(s): Department of Material Science and Engineering, Cornell University

Primary Source(s) of Research Funding: Intel

Contact: cko3@cornell.edu, fhk28@cornell.edu, cw867@cornell.edu
Website(s): https://ober.mse.cornell.edu/

Primary CNF Tools Used: ASML 300C DUV Stepper, AFM Bruker Icon, JEOL 6300 E-Beam, Woollam RC2, Zeiss Ultra SEM, YES HMDS prime oven

Abstract:

Polymeric photoresists are limited in sensitivity, resolution, and line-edge roughness largely due to their various molar mass distributions and polymer chain compositions. Polypeptoids are, however, characterized by low stochastics. In this work we describe the synthesis of ten repeating-unit polypeptoids designed as photopolymers and demonstrate their potential as chemically amplified resists (CARs) evaluated by electron-beam (E-Beam), deep ultraviolet (DUV) and extreme-ultraviolet lithography (EUVL), obtaining well-defined line-space patterns of less than 30 nm half-pitch.

Summary of Research:

While in the last decade there has been significant progress on the design and synthesis of resists for EUVL, shortcomings of these resists still exist [1-3]. Despite the novel inorganic and metal-organic systems with good lithographic performance, their design is limited by their molecular structure [4]. For polymeric resist, their intrinsic defects always limit their lithographic performance [5]. In this work, we demonstrate the synthesis of polypeptoids whose structure, molecular weight, composition, and microstructure can be precisely controlled via a sequence-defined synthetic method [6-8] and investigate their potential as resists for EUVL.

Several libraries of polypeptoid with ten repeating units were synthesized. In particular we focus on four polypeptoids of which the sequences were altered, see Figure 1. After synthesis the polypeptoids were characterized by differential scanning calorimetry (DSC) to determine the glass transition temperature, and matrix assisted laser desorption ionization time-of-flight mass spectrometry (MALDI-TOF) was applied to confirm the polypeptoid structure, as previously reported [7]. Di-*tert*-butyl decarbonate (tBOC) was used to protect the hydroxy groups to introduce solubility-switch ability. By introducing short aliphatic and bulky sidechains, we were able to further tailor the solubility and contrast and obtained a resist which is developable in dilute aqueous base. Furthermore, polypeptoids with chain-end hydrophobic sidechains presented a better lithographic. This is attributed to microstructure and the increasing chain-mobility.

The lithographic performance of the synthesized polypeptoids was evaluated by E-Beam lithography. The best performing scanning electron microscope (SEM) micrographs represent the polypeptoid with a block-like structure where the short aliphatic and bulky aromatic sidechains are placed at the termini of the polypeptoid chain, see Figure 2.

Figure 3 shows the EUVL contrast curve taken from Paul-Scherrer Institute (PSI) in Switzerland, which presents a clearing dose at around 10 mJ/cm^2 indicating a positive tone, sensitive resist, while the change in sequence did not significantly affect the dosage to clear. It is worth noting that our first experiments indicated that a change of tone occurs by aging the resist solution. This might be attributed to the stability of the carbonate protecting group, which is reduced by terminal carboxylic acids of the polypeptoid chain. However, further studies are required to better understand the effect of the end-groups of the polypeptoids on solution stability and lithographic performance.

Conclusions and Future Work:

In this work we demonstrate the synthesis of short polypeptoids and show their potential as resists for EUVL. By introducing hydrophobic-aliphatic and aromatic bulky sidechains the solubility change could be tailored to obtain an aqueous-base developable resist. While the compositions of the synthesized polypeptoids were the same, the sequence was varied, affecting the lithographic performance. However, the best performance was observed placing the hydrophobic moieties closer to the chain ends, forming a symmetrical segmented structure, obtaining line: space patterns of 36 nm half-pitch by E-Beam lithography. The clear dosage of the best performing EUV resist was determined to be about 10 mJ/cm^2 showing a sharp change in solubility with increasing dosage. While we could successfully show the potential application of these materials as EUV resist, further research is required to optimize the lithographic performance, improve the stability in solution and identify the effect of sequence on lithographic patterning.

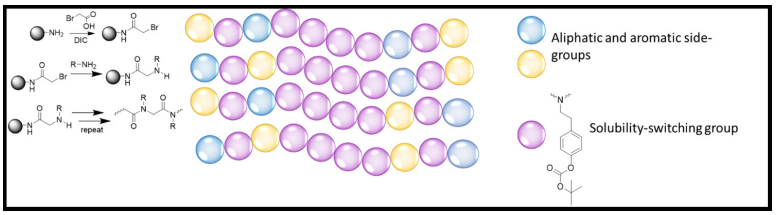

Figure 1: Solid phase supported synthesis of four different sequences of polypeptoid with short hydrophobic aliphatic and bulky aromatic side chains.

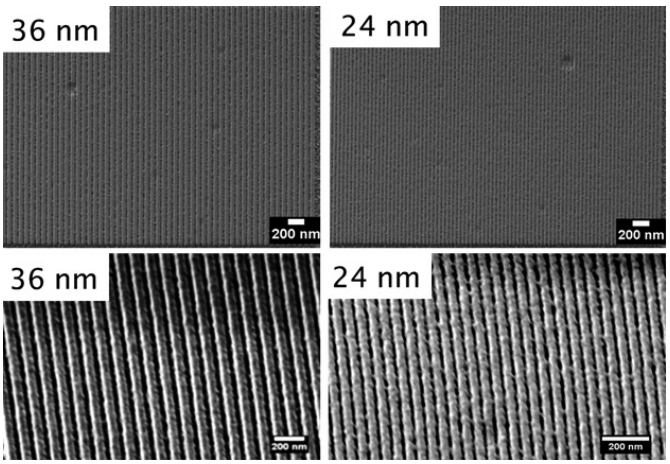

Figure 2: Electron-beam 1:1 line: space micrographs of the best performing polypeptoid developed in dilute 0.1 TMAH aqueous solution for 20s. PAG: TPS-PFBS (20 wt.%), Dosage: 216μC/cm^2.

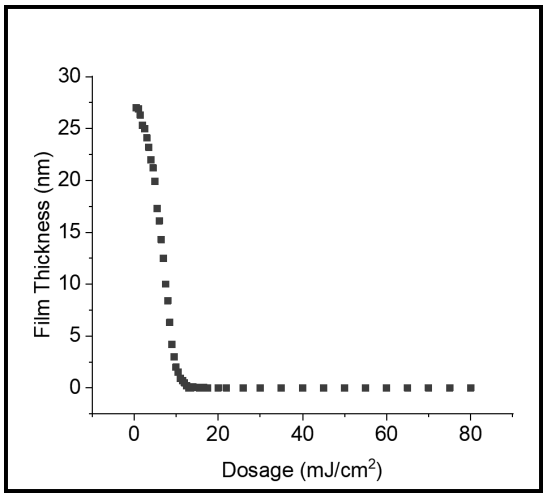

Figure 3: EUV contrast curve of a block-like polypeptoid with a short aliphatic and bulky aromatic sidechain at both termini.

References:

[1] Lio, A., "EUV Photoresists: A Progress Report and Future Prospects," Synchrotron Radiation News, 32(4): p. 9-14 (2019).

[2] Li, L., et al., "Extreme ultraviolet resist materials for sub-7 nm patterning," Chemical Society Reviews, 46(16): p. 4855-4866, (2017).

[3] Manouras, T. and P. Argitis, "High Sensitivity Resists for EUV Lithography: A Review of Material Design Strategies and Performance Results," Nanomaterials (Basel), 10(8) (2020).

[4] Luo, C., et al., "Review of recent advances in inorganic photoresists," RSC Advances, 10(14): p. 8385-8395, (2020).

[5] Anna, L. "EUV resists: What's next?," in Proc.SPIE, (2016).

[6] Deng, J., et al., "New Approaches to EUV Photoresists: Studies of Polyacetals and Polypeptoids to Expand the Photopolymer Toolbox," Journal of Photopolymer Science and Technology, 34(1): p. 71-74, (2021).

[7] Meng, X.Z., et al. "Controlled sequence peptoids as photoresist platforms for high-resolution DUV/EUV photoresists, "Proc. SPIE, (2022).

[8] Florian Kaefer, Z.M., Rachel Segalman, Christopher Ober. "Controlled Sequence Photoresists from Polypeptoids," The 39th International Conference of Photopolymer Science and Technology, (2022).

Micro-Etched Sorbent SPMESH Sheets for High Throughput, Trace-Level Analysis of "Smoke Taint" Compounds in Grapes and Wines

CNF Project Number: 2513-16
Principal Investigator(s): Gavin Sacks
User(s): Terry Bates, Austin Montgomery, Heather Scott, Andy Kalenak

Affiliation(s): Department of Food Science, Cornell University
Primary Source(s) of Research Funding: New York Wine and Grape Foundation
Contact: gls9@cornell.edu, tlb247@cornell.edu, am3253@cornell.edu, has224@cornell.edu, apk66@cornell.edu
Website(s): http://blogs.cornell.edu/winechemistry/
Primary CNF Tools Used: VersaLaser Engraver/Cutter Tool

Abstract:

Exposure of grapes to the smoke of forest or brush fires may result in "smoky" off-aromas ("smoke taint") in resulting wines due to several odorants, including volatile phenols like cresol and guaiacol. These volatile phenols are detectable at low ppb (ng/g) concentrations, and their analysis typically requires lengthy analyses (20-40 min) by gas chromatography - mass spectrometry (GC-MS). The slow analytical throughput of GC-MS creates bottlenecks during smoke exposure events during harvests, and limits the ability of vineyards and wineries to make data-driven decisions. Using tools available through the Cornell NanoScale Facility (CNF), we have prepared etched sorbents sheets ("SPMESH") designed for selective extraction of volatile phenols. The sheets are designed to fit over multiwell plates and allow for parallel extraction of odorants prior to rapid mass spectrometric analysis. The optimized method can analyze 24 samples in < 10 min, or nearly a 100-fold improvement in throughput over the gold standard method.

Summary of Research:

SPMESH sheets were prepared by etching a grid pattern in thin silicone sheets using the VersaLaser Cutter/Engraver at CNF, using a previously described protocol (Figure 1, left) [1]. SPMESH sheets were positioned over multiwell plates containing wine or grape samples to extract volatile phenols from the sample headspace. Extracted sample sheets were then analyzed by direct analysis in real time mass spectrometry (DART-MS) (Figure 1, right). Poor signal response and detection limits (>1 mg/L) were initially observed. This was determined to be due to the high polarity of the analytes. This problem was addressed by derivatization with deuterated acetic anhydride (Figure 2). The full workflow is shown in Figure 3.

Following optimization, figures of merit were determined in juice and wine. Detection limits for target compounds were ~ 1 μg/L for the three target VPs, below sensory threshold. Good linearity and reproducibility were also achieved. The DART-MS analysis requires < 10 min to analyze 24 samples, or about 50-100 faster than gas chromatography-mass spectrometry (GC-MS), the current gold standard. Including derivatization and extraction time, the entire approach requires ~ 60 min for 24 samples. For validation, juice and wine samples were sourced from an industry cooperator. Samples were analyzed by both the new SPMESH-DART-MS method and the gold standard GC-MS method. Good agreement was observed between the two methods for all analytes (r2 = 0.7-0.9). Results of the work have been published ([2] Bates and Sacks, 2023) and the approach is being shared with commercial fee-for-service analytical labs.

References:

[1] Bee, Madeleine Y., Jillian A. Jastrzembski, and Gavin L. Sacks. "Parallel headspace extraction onto etched sorbent sheets prior to ambient-ionization mass spectrometry for automated, trace-level volatile analyses." Analytical chemistry 90.22 (2018): 13806-13813.

[2] Bates, Terry L., and Gavin L. Sacks. "Rapid headspace solid-phase microextraction sheets with direct analysis in real time mass spectrometry (SPMESH-DART-MS) of derivatized volatile phenols in grape juices and wines." Analytica Chimica Acta (2023): 341577. https://www.sciencedirect.com/science/article/pii/S0003267023007985.

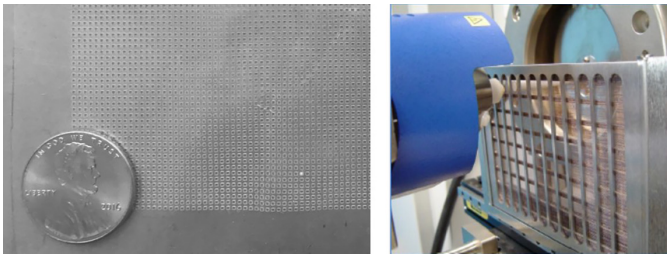

Figure 1: (left) Etched silicone SPMESH sheet produced at the CNF. The grid size is 0.5 mm × 0.5 mm, and (right) SPMESH sheet positioned during DART-MS analysis.

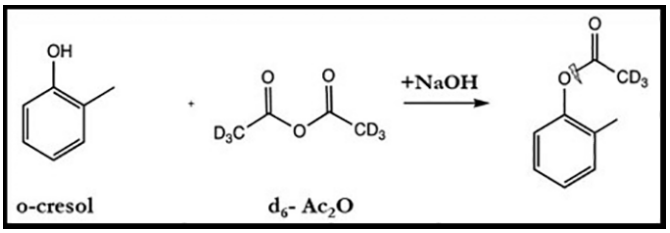

Figure 2: Acetylation scheme used to increase hydrophobicity and extractability of targeted phenols.

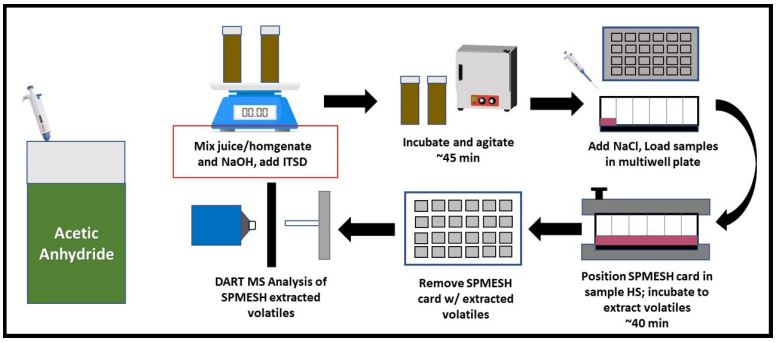

Figure 3: Workflow for rapid analyses of "smoke taint" odorants (volatile phenols) in grapes and wines.

Identifying the Occurrence and Sources of Per- and Polyfluoroalkyl Substances in Photolithography Wastewater

CNF Project Number: 2938-21
Principal Investigator(s): Damian Helbling[1], Christopher Kemper Ober[2]
User(s): Paige Jacob[1]

Affiliation(s): 1. Civil and Environmental Engineering, 2. Materials Science & Engineering; Cornell University
Primary Source(s) of Research Funding: Semiconductor Research Corporation and National Science Foundation
Contact: deh262@cornell.edu, cko3@cornell.edu, pvj7@cornell.edu
Website(s): https://helbling.research.engineering.cornell.edu/
Primary CNF Tools Used: DISCO Dicing Saw, Jelight 144AX UVO-Cleaner, FilMetrics F40

Abstract:

Per- and polyfluoroalkyl substances (PFASs) are contaminants of concern to environmental and human health [1]. PFASs are present in photolithography materials [2] and might undergo transformation reactions during photolithography. We acquired five photolithography materials and characterized the occurrence of organic fluorine and PFASs in the materials. We performed photolithography experiments, collected the wastewater samples for subsequent analyses, and used a mass balance approach to assess the extent of transformations. The goal of the project was to evaluate the evolution of fluorinated materials during photolithography to gain an improved understanding of whether photolithography is a major source PFASs in fabrication (fab) wastewater.

Chemical	Measured TF	Measured AOF	% of Solid Components as TF	% TF captured by AOF
Photoresist A	1.65±0.14	0.37±0.04	1.65±0.14	22.3±1.93
Photoresist B	0.36±0.03	0.18±0.00	0.55±0.04	51.8±3.67
Photoresist C	1.31±0.04	0.68±0.08	0.65±0.02	52.0±7.25
TARC A	18.1±0.35	2.38±0.27	60.2±1.12	13.2±1.70
TARC B	4.62±0.08	0.62±0.06	15.4±0.27	13.4±1.19

Table 1: Average and standard deviation of total fluorine (TF) and adsorbable organic fluorine (AOF) concentrations (g L-1) conducted by means of combustion ion chromatography (CIC) in the five photolithography materials prior to photolithography.

Summary of Research:

A variety of PFASs and fluoropolymers are used in photolithography materials and a recent study demonstrated that fab wastewater contains PFASs [4]. Although it is known that perfluorobutane sulfonate (PFBS) is a widely used constituent of photoacid generators (PAGs) [2], the sources of nearly all other PFASs in fab wastewater remain unknown.

Constituents of photolithography materials are also subject to transformation reactions induced by the conditions of photolithography, which expose the materials to UV radiation and highly basic conditions [5]. We hypothesize that a major source of PFASs in fab wastewater are PFASs used or generated during photolithography. We acquired five photolithography materials and designed experiments to: (1) characterize the organic fluorine and PFAS in the materials; and (2) assess the formation or destruction of PFASs during photolithography.

We acquired three photoresists (Photoresists A, B, and C) and two top antireflective coatings (TARCs A and B). We measured the total fluorine (TF) of the materials, which ranged between 0.36 - 18.1 g L-1 (Table 1). We also measured the adsorbable organic fluorine (AOF) of the materials, which ranged from 0.18 - 2.38 g L-1 (Table 1), confirming that the materials have organofluorine-containing constituents.

We performed a target analysis for 39 PFASs in the materials. In Photoresist A and Photoresist C, we identified PFBS at 581±50 mg L-1 and 470±104 mg L-1, respectively, and the fluorine from PFBS accounts for 20% of the TF in both materials. PFBS was the only target PFAS that can explain a significant portion of the TF in these two materials. In an effort to identify other PFASs that could contribute to the TF, we performed suspect and nontarget analyses. We identified 20 suspect PFASs in TARC A and found that these PFASs explained 17.0±13.8% of the TF in TARC A. No other suspect or nontarget PFASs were found in the other materials. After applying target, suspect, and nontarget screenings, 80% of the TF in Photoresist A and C, 92% of the TF in TARC A, and approximately 99% of the TF in Photoresist B and TARC B remains uncharacterized. We suspect that the remaining TF can be attributed to fluorine present in polymeric form.

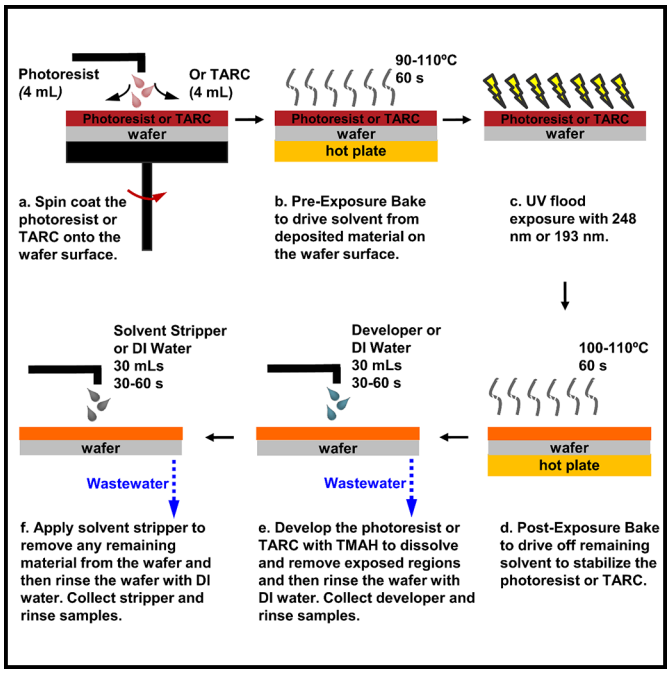

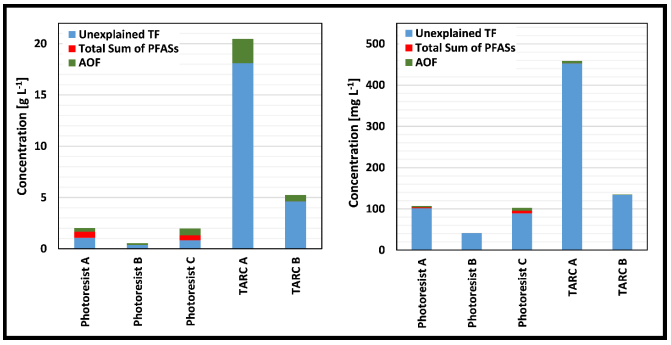

Figure 1, top: Photolithography process diagram detailing specific experimental parameters of each step. The exact parameters applied at different steps (i.e., spin coating and baking) were adjusted for each material according to the specifications provided by the manufacturers.

Figure 2, below: (a) Concentrations in g L-1 of unexplained total fluorine (TF), measured adsorbable organic fluorine (AOF), and the amount of TF that is attributed to the total sum of target PFASs measured in the materials. (b) Concentrations in mg L-1 of unexplained total fluorine (TF), measured adsorbable organic fluorine (AOF), and the amount of TF that is attributed to the total sum of target PFASs measured in the 248 nm wastewater samples. We note the different units used on the y-axis in (a) and (b) that reflect dilution of each material during the photolithography experiments.

We performed photolithography experiments and collected the wastewater from each material after development and stripping (Figure 1). We performed TF and AOF analyses and target, suspect, and nontarget screenings on the wastewater samples to identify the PFASs present post-photolithography. These measurements allowed us to track the mass of the materials throughout photolithography.

The wastewater samples generated contained no measurable TF. We surmise that a combination of TF loss during spin coating and subsequent dilution in the wastewater samples resulted in concentrations that were below the method limit of quantification. Next, we measured the AOF of the wastewater samples which ranged from 126.7 - 6976.7 ug L-1.

We performed a target screening on the wastewater samples and determined the extent of formation or destruction of the target PFASs by implementing a mass balance approach. These mass balance analyses indicate that target PFASs were being created or destroyed to some extent during photolithography, but that the changes in masses fail to explain more than 1% of the TF of each material. Over 75% of the TF of each material remains unexplained after these mass balance analyses indicating the stability of the organofluorine-containing constituents (e.g., fluoropolymers) of these materials during photolithography [2]. We also applied the suspect and nontarget screening workflows on the samples.

We discovered 13 suspect or nontarget PFASs unique to the wastewater of each material and exposure but expect that none of these compounds would contribute greater than 1% to the measured TF.

Conclusions and Future Steps:

We conclude that: (1) the selected photoresists and TARCs have organofluorine-containing compounds at similar levels of other industrial and commercial products and formulations; (2) target PFASs present in these materials can only explain up to 20% of the TF in a material; and (3) the simulated photolithography experiments did not induce significant transformations. This study highlights the complexity of tracking the source of PFASs in a fab, as the simulated photolithography experiments did not yield the expected results.

Future steps will focus on evaluating the fate and transformation of fluoropolymers during photolithography and wastewater treatment.

References:

[1] Z. Wang, et al.; 10.1021/acs.est.6b04806.
[2] C. K. Ober, et al.; 10.1117/1.JMM.21.1.010901.
[3] C. A. McDonough, et al.; 10.1016/j.coesh.2018.08.005
[4] P. Jacob, et al.; 10.1021/acs.est.0c06690.
[5] D. Bratton, et al.; 10.1002/pat.662.

Scalable Defect Engineering in Metal-Organic Frameworks via High-Concentration Self-Assembly Utilizing Pre-Assembled Cluster Precursors

CNF Project Number: 2996-21
Principal Investigator(s): Phillip J. Milner
User(s): Ronald T. Jerozal

Affiliation(s): Department of Chemistry and Chemical Biology, Cornell University

Primary Source(s) of Research Funding: National Institute of General Medical Sciences of the National Institutes of Health under award number R35GM138165

Contact: pjm347@cornell.edu, rtj32@cornell.edu

Website(s): https://blogs.cornell.edu/milner/

Primary CNF Tools Used: Rame-Hart 500 Goniometer

Abstract:

Metal-organic frameworks (MOFs) are a class of porous, crystalline materials that can have tailored properties based on the incorporation of defects and are promising for applications in gas storage, catalysis, and separations. Syntheses of MOFs on large scale, however, remain a major roadblock to their further implementation, as many are synthesized using solvothermal methods under highly dilute (≤0.01 M) conditions. Additionally, a large excess (>50 equiv.) of competing acid modulators is often used to enhance the crystallinity of and the number of defects in the resulting MOF, further amplifying the associated waste of MOF synthesis. We demonstrated that zirconium and hafnium MOFs are generally able to be synthesized at much higher reaction concentrations (up to 1.0 M). Additionally, the use of pivalate-capped metal cluster precursors — as opposed to a standard metal chloride salt — led to the inclusion of pivalate defects at missing-linker sites, which increased the hydrophobicity of the resulting MOF. Our findings provide a user-friendly approach to the scalable synthesis of defect engineered MOFs by drastically reducing solvent and acid modulator waste.

Summary of Research:

Metal-organic frameworks (MOFs) are crystalline, porous solids constructed from inorganic nodes bridged by organic linkers [1]. MOFs are promising for a variety of applications, including heterogeneous catalysis, gas storage, and chemical separations, due to their highly tunable pores that can resist collapse upon desolvation [1]. The controlled incorporation of defects in MOFs, such as missing-linker defects, can be utilized to tune the resulting framework properties by further modifying the size and chemical functionality of the pores [2]. Despite their potential, a major challenge to the further development of MOFs is their synthesis on bench top scales (1-100g). This is mostly due to the excessive waste generated during synthesis as many use very dilute (~0.01M) solvothermal conditions in hazardous solvents such as dimethylformamide (DMF) [3]. Additionally, many syntheses use a staggering excess (>50 equiv.) of competing acid modulators to enhance the crystallinity of and to increase the number of defects in the resulting MOFs [1]. These synthetic challenges are exemplified by frameworks composed of zirconium (Zr) and hafnium (Hf) cluster nodes, such as UiO-66 (UiO = Universitetet i Oslo) (Figure 1). Zr-and Hf-MOFs display exceptional tunability, hydrolytic stability, and robust structures that can accommodate large amounts of defects but often require dilute synthesis conditions and large amounts of modulators to yield crystalline products [1].

Recently, we reported that Zr-and Hf-MOFs can generally be self-assembled at much higher reaction concentrations (up to 1.0 M) than traditionally utilized [4]. By simply combining stoichiometric amounts of terephthalic acid (H_2bdc) linker and $ZrCl_4$ in DMF at concentrations up to 1.0 M, crystalline UiO-66 (labeled UiO-66-1.0M ($ZrCl_4$)) was obtained (Figure 2). Likewise, a pivalate-capped Zr_6 cluster (ZrPiv) could be combined with stoichiometric H_2bdc and hydrochloric acid (HCl) — to promote ligand exchange of pivalates for linkers — to yield crystalline MOF labeled UiO-66-1.0M (ZrPiv) (Figure 2). These high-concentration samples displayed similar crystallinity to a dilute prepared sample and had Brunauer-Emmett-Teller (BET) surface areas comparable to literature values [4]. A key difference, however, was that UiO-66-1.0M (ZrPiv) contained pivalate ligands as linker substitution defects. Proton nuclear magnetic resonance (1H NMR) analysis was used to determine a pivalate:linker ratio of 0.11:1, which is comparable to reported dilute syntheses of UiO-66 that use a slight excess of competing carboxylic acid modulators. Additionally, this ratio was higher than for a

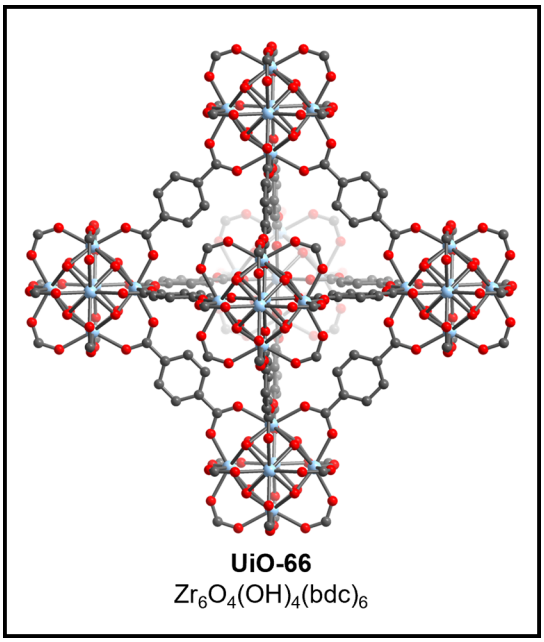

Figure 1: The structure of UiO-66. Gray, red, and light blue spheres represent carbon, oxygen, and zirconium, respectively. Hydrogens are omitted for clarity.

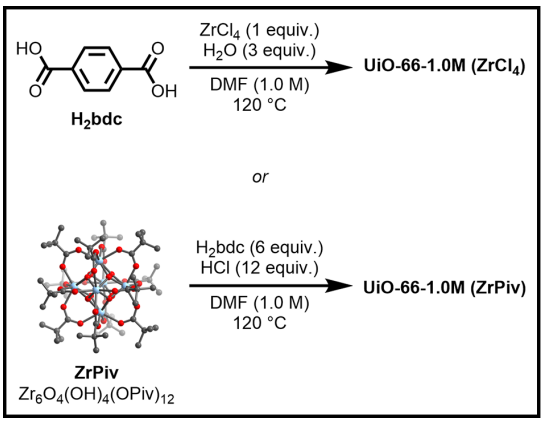

Figure 2: High-concentration synthesis of UiO-66 from either $ZrCl_4$ or ZrPiv. Adapted with permission from ref [4]. Copyright 2023 American Chemical Society.

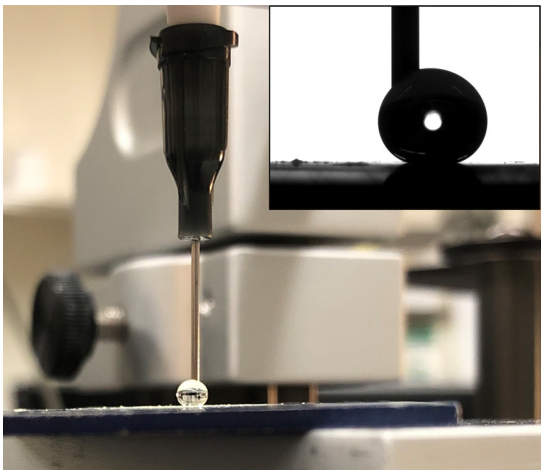

Figure 3: Photo of a water drop on UiO-66-1.0M (ZrPiv) powder. Inset: water contact angle of UiO-66-1.0M (ZrPiv). Adapted with permission from ref [4]. Copyright 2023 American Chemical Society.

sample prepared at high concentrations using $ZrCl_4$ and the same amount of pivalic acid present in ZrPiv [4]. Thus, using ZrPiv as a precursor is more effective at carboxylate defect incorporation than traditional acid modulation in high-concentration syntheses.

We hypothesized that UiO-66-1.0M (ZrPiv) should have enhanced hydrophobicity due to the inclusion of nonpolar pivalate defects. When water is added to the pivalate containing MOF, it beads up indicating that the material has a hydrophobic surface (Figure 3). Water contact angle measurements determined that UiO-66-1.0M (ZrPiv) had a large contact angle of 162° (Figure 3 inset), which indicates this as a super-hydrophobic surface [4].

Additionally, UiO-66-1.0M (ZrPiv) floats on water whereas UiO-66-1.0M ($ZrCl_4$) is rapidly wetted and sinks (Figure 4 inset). Water vapor adsorption isotherms were also measured to further probe if the interior pore surface of the pivalate containing MOF showed enhanced hydrophobicity (Figure 4). The relative pressure at which half of the total water capacity is reached (α) is larger for UiO-66-1.0M (ZrPiv) ($\alpha = 0.30$) indicating that its pore surface has weaker interactions with adsorbed water than UiO-66-1.0M ($ZrCl_4$) ($\alpha = 0.24$) [4]. Overall, these results demonstrate that preformed cluster precursors can effectively install property altering defects and thus enable defect engineering in user-friendly high-concentration MOF synthesis.

References:

[1] Bai, Y.; Dou, Y.; Xie, L.-H.; Rutledge, W.; Li, J.-R.; Zhou, H.-C. Zr-Based Metal-Organic Frameworks: Design, Synthesis, Structure, and Applications. Chem. Soc. Rev. 2016, 45 (8), 2327-2367. https://doi.org/10.1039/C5CS00837A.

[2] Feng, Y.; Chen, Q.; Jiang, M.; Yao, J. Tailoring the Properties of UiO-66 through Defect Engineering: A Review. Ind. Eng. Chem. Res. 2019, 58 (38), 17646-17659. https://doi.org/10.1021/acs.iecr.9b03188.

[3] Julien, P. A.; Mottillo, C.; Fri..i., T. Metal-Organic Frameworks Meet Scalable and Sustainable Synthesis. Green Chem. 2017, 19 (12), 2729-2747. https://doi.org/10.1039/C7GC01078H.

[4] Jerozal, R. T.; Pitt, T. A.; MacMillan, S. N.; Milner, P. J. High-Concentration Self-Assembly of Zirconium-and Hafnium-Based Metal-Organic Materials. J. Am. Chem. Soc. 2023, 145 (24), 13273-13283. https://doi.org/10.1021/jacs.3c02787.

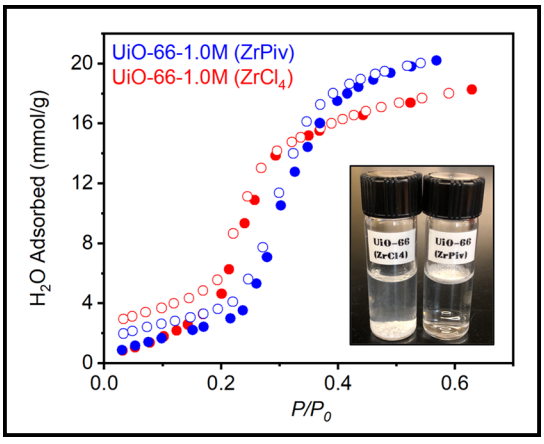

Figure 4: Water vapor adsorption isotherms of high-concentration UiO-66 samples. Inset: UiO.66-1.0M (ZrPiv) (right) floating on water vs. UiO-66-1.0M ($ZrCl_4$) (left) sinking in water. Adapted with permission from ref [4]. Copyright 2023 ACS.